

## SYNTHESIS AND CHARACTERIZATION OF TiO<sub>2</sub> NANOPOWDERS FOR FABRICATION OF DYE SENSITIZED SOLAR CELLS

T. PHONKHOKKONG<sup>a</sup>, T. THONGTEM<sup>b,c</sup>, S. THONGTEM<sup>a\*</sup>,  
A. PHURUANGRAT<sup>d</sup>, W. PROMNOPAS<sup>a</sup>

<sup>a</sup>*Department of Physics and Materials Science, Faculty of Science, Chiang Mai University, Chiang Mai 50200, Thailand*

<sup>b</sup>*Department of Chemistry, Faculty of Science, Chiang Mai University, Chiang Mai 50200, Thailand*

<sup>c</sup>*Materials Science Research Center, Faculty of Science, Chiang Mai University, Chiang Mai 50200, Thailand*

<sup>d</sup>*Department of Materials Science and Technology, Faculty of Science, Prince of Songkla University, Hat Yai, Songkhla 90112, Thailand*

Titanium dioxide (TiO<sub>2</sub>) nanopowders were synthesized by sol-gel and refluxing methods, and compared with commercial titanium dioxide (P25). The as-synthesized TiO<sub>2</sub> samples were characterized by X-ray diffraction, Raman spectroscopy, scanning and transmission electron microscopy, energy dispersive X-ray (EDX) spectroscopy, selected area electron diffraction (SAED), and UV-vis and photoluminescence (PL) spectroscopy. In this research, the as-synthesized samples were used to fabricate dye sensitized solar cells (DSSCs) and found that TiO<sub>2</sub> synthesized by sol-gel method has the highest efficiency of  $V_{OC} = 0.465$  V,  $J_{SC} = 1.361$  mA/cm<sup>2</sup> and FF = 0.647.

(Received November 18, 2015; Accepted January 13, 2016)

**Keywords:** Nanopowder; Sol-gel; Titanium dioxide; Dye sensitized solar cells

### 1. Introduction

TiO<sub>2</sub> nanostructures in various forms are finding wider applications than before because of their specifically size-related properties. The energy band structure becomes discrete for nanometer-scale TiO<sub>2</sub>. Its photophysical, photochemical, and surface properties are quite different from those of the bulks due to the quantum size effect [1]. A number of methods have been used to prepare TiO<sub>2</sub> nanoparticle: chemical precipitation, microemulsion, hydrothermal reaction, sol-gel and refluxing [2]. Sol-gel processing of titanium dioxide has been extensively investigated and modern processes have been developed to refine and control the stability and phase formation of the colloidal precursor [3]. Reflux involves heating reaction for a specific amount of time, and continually cooling the produced vapor back into liquid form through a condenser. The vapors produced above the reaction continually undergo condensation, returning to the flask as a condensate. The reaction temperature remains constant [4]. To synthesize TiO<sub>2</sub> by refluxing and sol-gel method, the easiest developed methodology consists the use of a mixture of titanium (IV) alcoxide precursor and preform TiO<sub>2</sub> nanoparticles. This route has the difficulty of controlling the degree of alcoxide hydrolysis. In a similar approach, the titanium molecular precursor is replaced by small size titania nanoparticles (<10 nm) that act as a glue due to its great tendency to aggregate and to get anchored to the larger titania nanoparticles [5]. In the present work, the structural and optical properties of amorphous and crystalline nanostructured TiO<sub>2</sub> powders were investigated and compared with those of the commercial one. The obtained sol-gel and reflux TiO<sub>2</sub> was annealed at 400 °C [6]. Among these techniques, the sol-gel process is currently recognized as one of the most important chemical technique for the synthesis of TiO<sub>2</sub> nanoparticles, due to several

---

\*Corresponding author: schthongtem@yahoo.com

advantages: low processing temperature, versatile processing, high homogeneity and stability [7,8]. In the presence of higher amounts of water, high hydrolysis rates are desired for the formation of  $\text{Ti}(\text{OH})_4$ , which condense to yield  $\text{Ti}-\text{O}-\text{Ti}$  chains. The excess water suppresses the development of  $\text{Ti}-\text{O}-\text{Ti}$  species, because chemical equilibrium causes the favorable creation of  $\text{Ti}-\text{OH}$  species [9]. Calcination temperature is especially important for removing organic molecules from the final products and completing the crystallization. Moreover, very high calcination temperature results in aggregation, phase transformation and the properties of  $\text{TiO}_2$  nanoparticles are required.

In this study  $\text{TiO}_2$  was synthesized by the sol-gel and reflux methods under synthesis condition to achieve the  $\text{TiO}_2$  nanopowder with high anatase content. The two methods were performed for comparison with commercial  $\text{TiO}_2$  (P25). The effect on the powder size of  $\text{TiO}_2$  with a small size and narrow distribution was studied and the products were characterized by different methods.

## 2. Experimental procedure

### Chemicals

All chemicals used in this experiment were titanium (IV) oxide (P25) anatase nanopowder < 25 nm particle size 99.7%, Fluka Analytical; Titanium (IV) butoxide,  $\text{Ti}(\text{OBu})_4$ ,  $\text{C}_{16}\text{H}_{36}\text{O}_4\text{Ti} \geq 97\%$ ; I-Propanol ( $\text{C}_3\text{H}_8\text{O}$  99.5%, QRCC); Acetyl acetone (acac,  $\text{CH}_3\text{CO}.\text{CH}_2.\text{CO}.\text{CH}_3$ , 99% BDH laboratory Supplies); Ethanol (EtOH, 95%); Nitric acid ( $\text{HNO}_3$ , 65%, Carlo Erba) and deionized water.

### Preparation of pure $\text{TiO}_2$

#### Sol-gel method

$\text{TiO}_2$  nanopowder was prepared by a sol-gel method [10] at room temperature as follows: 8.68 mL of titanium (IV) butoxide ( $\text{Ti}(\text{OBu})_4$ ) was dissolved in a mixture solution of 35 mL of EtOH 0.05 mol complexing agent. After magnetic stirring for 2 h, the obtained solution was hydrolyzed by the addition a mixture of water and EtOH dropwise under stirring for another 2 h. The white precipitate has been washed with ethanol and double distilled water and dried at 100 °C for 3 h and annealed at 400 °C in air for 2 h.

#### Refluxing method

$\text{TiO}_2$  was prepared using a refluxing method with some modification [2]. Titanium (IV) butoxide, ( $\text{Ti}(\text{OBu})_4$ ), in I-Propanol was used as molecular precursor of  $\text{TiO}_2$ . The molar ratio of these reactants was  $\text{Ti}(\text{OBu})_4:\text{H}_2\text{O}:\text{I-Propanol}:\text{acac} = 1:100:2:0.01$ . In order to control the reaction kinetics, acetyl acetone was used as a chemical additive to moderate the reaction rate. The deionized water used for hydrolysis in solution with I-Propanol was added gradually under mechanical stirring for 4 h to form titanium oxyhydroxide, which was then washed with water for several times. The final solution containing  $\text{HNO}_3$  (pH of 1-2.5) was refluxed at 85 °C for 8 h. The precipitate of titanium oxyhydroxide was dried at 100 °C for 3 h, and annealed at 400 °C for 2 h.

### Preparation of $\text{TiO}_2$ films

For  $\text{TiO}_2$  film preparation,  $\text{TiO}_2$  nanopowder prepared by different methods: commercial  $\text{TiO}_2$  (P25), reflux method and sol-gel method were prepared by dissolving 0.1 M nitric acid ( $\text{HNO}_3$ , 65%) in deionized water followed by stirring at room temperature for 3 h. Finally, a homogeneous and colorless solution was obtained. Ratio of  $\text{TiO}_2$  nanopowder : nitric acid was 0.5 g : 10 ml. FTO substrates were cleaned in an ultrasonic bath with acetone and ethanol solution. A scotch tape was put on the conducting side of FTO.  $\text{TiO}_2$  films were deposited on top by doctor-blade method. The as-produced films were annealed at 450 °C with a heating rate of 5 °C/min for 2 h to eliminate the organic residues. Textured film prepared from P25, synthesis protocol reflux and sol-gel were named as film A, film B and film C, respectively.

### Fabrication of DSSCs

The TiO<sub>2</sub> films were immersed in a 0.5 mM N719 dye-acetonitrile solution at room temperature for different lengths of time, ranging from 30 min to 1 h. The Pt-coated films as counter electrodes were fabricated by dropping 20 mM chloroplatinic acid in acetone on the FTO substrates, followed by heating at 550 °C for 1 h. The TiO<sub>2</sub> films were modified as dye-loaded photoanodes and counter electrodes. Each sandwich cell was held in place by two heavy-duty clips on opposite ends. The liquid electrolyte of 0.3 mol LiI and 0.03 mol I<sub>2</sub> in acetonitrile was introduced to one edge of each sandwich across an active area of 0.20 cm<sup>2</sup> [11].

### Characterization

The structural characterization of the nanoparticles was carried out by X-ray diffraction (XRD, SIEMENS D500) operating at 20 kV 15 mA and using Cu K<sub>α</sub> line in combination with the database of the Joint Committee on Powder Diffraction Standards (JCPDS) [12], transmission electron microscopy (TEM, JEOL JEM-2010) operating at 200 kV accelerating voltage, a scanning electron microscope (SEM, JEOL JSM-6335F) equipped with an energy dispersive X-ray (EDX) analyzer operating at 15 kV and a Raman spectrometer (T64000 HORIBA Jobin Yvon) using a 50 mW and 514.5 nm wavelength Ar green laser. Photoluminescence (PL) was carried out using LS 50B Perkin Elmer spectrophotometer with 255 nm excitation wavelength of 20 μW LED light at room temperature. The band gaps of the nanoparticles were investigated by optical absorption studies carried out using a UV-Vis spectrophotometer (Lambda 25 PerkinElmer) over the 200-700 nm range.

## 3. Results and discussion

### Characterization

X-ray diffraction was performed to examine the nanostructured feature and crystallinity of the pure TiO<sub>2</sub> synthesized by sol-gel, refluxing and commercial P25. Fig. 1 shows the X-ray diffraction patterns of TiO<sub>2</sub> synthesized by sol-gel, refluxing and commercial P25. In this research, XRD patterns of all the samples correspond to anatase phase and some rutile phase of TiO<sub>2</sub>. XRD analysis of the samples synthesized by sol-gel, refluxing and P25 show the existence of crystalline phase: the anatase phase of diffraction peaks at  $2\theta = 25.27^\circ, 37.84^\circ, 48.08^\circ, 54.35^\circ, 62.70^\circ$  and  $68.88^\circ$  correspond to the (101), (103), (200), (105), (213) and (116) planes. The rutile phase diffraction peaks at  $2\theta = 27.42^\circ, 36.10^\circ, 41.07^\circ, 54.33^\circ$  and  $56.68^\circ$  corresponds to the (110), (101), (111), (211) and (220) planes. The peaks of the samples prepared by sol-gel and refluxing methods were similar to that observed for TiO<sub>2</sub> (P25).

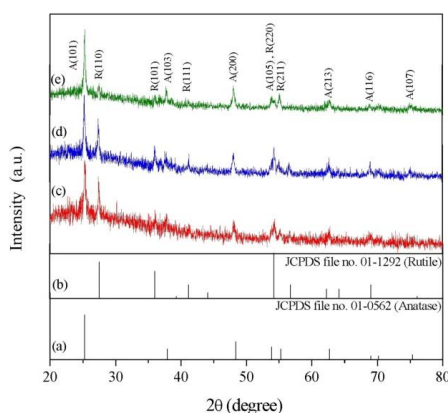


Fig. 1. XRD patterns of TiO<sub>2</sub> nanopowders prepared by different methods: (a) standard of TiO<sub>2</sub> anatase phase, (b) standard of TiO<sub>2</sub> rutile phase, (c) commercial TiO<sub>2</sub> (P25), (d) refluxing and (e) sol-gel.

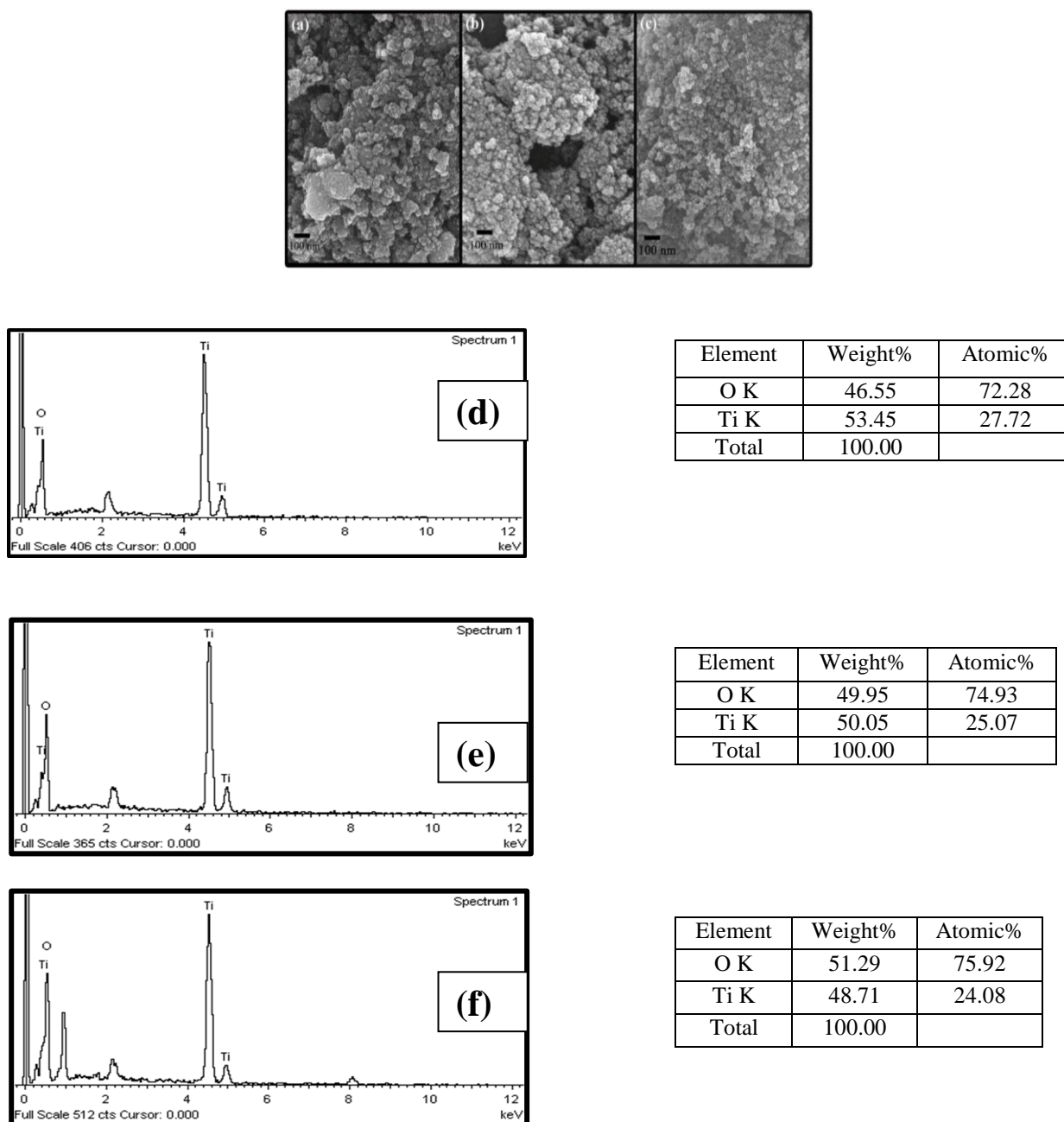


Fig. 2. SEM images and EDX spectra of  $\text{TiO}_2$  nanopowders prepared different methods: (a, d) sol-gel, (b, e) refluxing and (c, f) commercial  $\text{TiO}_2$  (P25).

Scanning electron microscopy (SEM) observation shows high homogeneity of the samples (Fig. 2(a–c)) prepared by the sol-gel, refluxing and commercial P25 with the average dimensions of about 40, 28 and 20 nm, respectively. The particle size calculated from the SEM images by the use of the Image J software. The particle size of  $\text{TiO}_2$  synthesized by sol-gel and refluxing methods were at the same size as the commercial nanopowder (P25) but the nanoparticles agglomerated as colonies with the size smaller than 50 nm. The particles were spherical and can be classified as: sol-gel > reflux > P25 in sequence (Fig. 3).

The elemental composition was determined by EDX analysis [13, 14], as the results shown in Fig. 2(d–f). The spectrum has prominent peaks of Ti and O, confirmed that the nanoparticles synthesized by sol-gel, refluxing and commercial P25 belong to pure  $\text{TiO}_2$ .

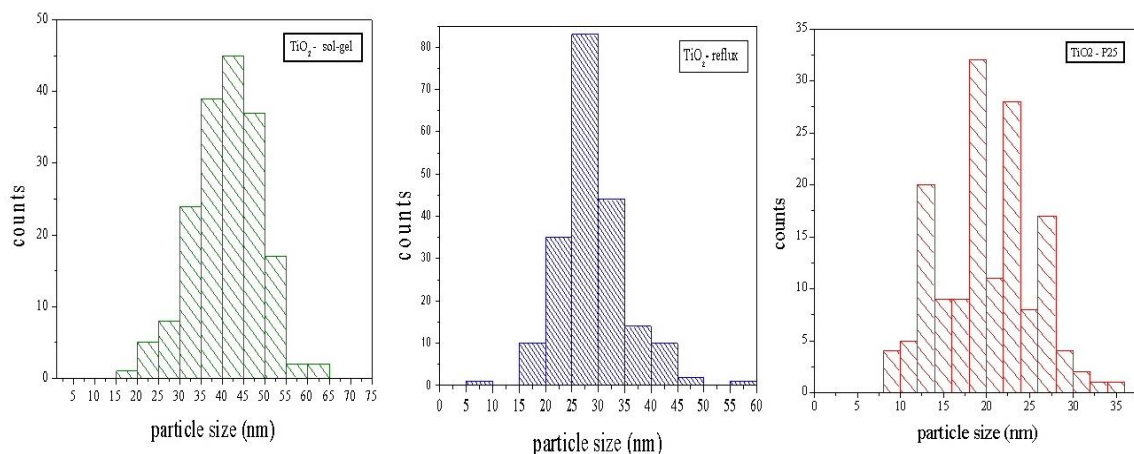


Fig. 3. Size distribution of  $\text{TiO}_2$  nanopowders prepared by different methods comparing with P25.

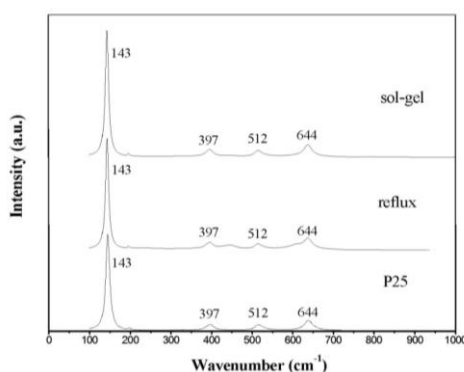


Fig. 4. Raman spectra of  $\text{TiO}_2$  nanopowders prepared by (a) sol-gel, (b) refluxing and (c) commercial P25.

Raman spectroscopy has also been applied to characterize the obtained  $\text{TiO}_2$  nanopowders, the phase purity of the  $\text{TiO}_2$  anatase and rutile was evident [15], as the results shown in Fig. 4. Anatase and rutile phase exhibit well distinct Raman finger print. The anatase structure is tetragonal. Its conventional cell is composed of two primitive one, each with two  $\text{TiO}_2$  units. Six modes are  $A_{1g}$  ( $517 \text{ cm}^{-1}$ ),  $2B_{1g}$  ( $397 \text{ cm}^{-1}$  and  $517 \text{ cm}^{-1}$ ) and  $3E_g$  ( $144 \text{ cm}^{-1}$ ,  $197 \text{ cm}^{-1}$  and  $640 \text{ cm}^{-1}$ ) are Raman active [15]. In this research, the products prepared by sol-gel, refluxing and commercial P25 show four peaks at 143, 397, 512 and  $644 \text{ cm}^{-1}$ , indicating the presence of  $\text{TiO}_2$  phase in accordance with above XRD results.

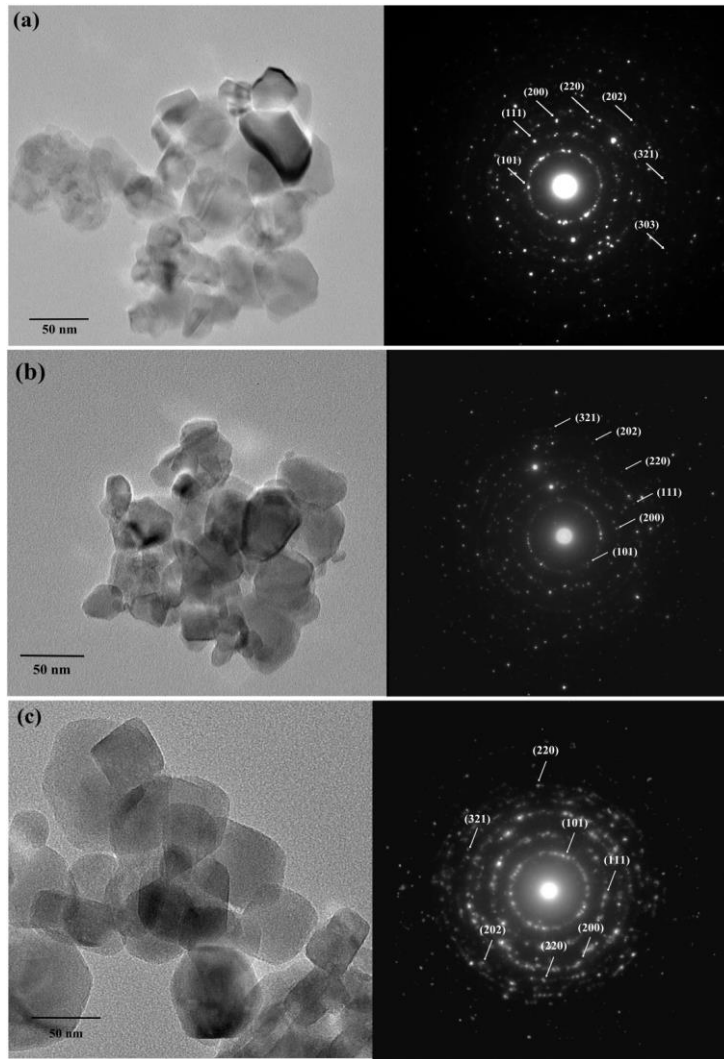


Fig. 5. TEM images and SAED patterns of  $\text{TiO}_2$  nanopowders prepared by (a) sol-gel, (b) refluxing and (c) commercial P25.

The TEM images of  $\text{TiO}_2$  nanopowders (Fig. 5) are for the products prepared by sol-gel, refluxing and commercial P25. These nanoparticles exhibit an obvious tendency of self-assembly into close-packed, dense, well-crystallized, almost uniform, unevenly size and irregular subnanoaggregates [16]. SAED patterns for  $\text{TiO}_2$  nanopowders prepared by sol-gel, refluxing and commercial P25 were indexed to correspond with the  $\text{TiO}_2$  phase.

In order to determine the nature of the band gap of  $\text{TiO}_2$  nanophase, UV-Vis absorption was characterized and the following relation is often used

$$(\alpha h\nu) = A(h\nu - E_g)^n \quad (1)$$

, where  $(h\nu)$  is the photon energy,  $E_g$  is the photonic band gap,  $\alpha$  is an absorption coefficient,  $A$  is a photonic-energy independent constant, and the value of  $n$  is  $1/2$  for direct transition. In this research, the absorbance and the plots of  $(\alpha h\nu)^2$  versus photon energy  $(h\nu)$  [17] are shown in Fig. 6. The photonic absorbance for the three samples shows the absorption of pure  $\text{TiO}_2$  prepared by sol-gel method at 280 nm, pure  $\text{TiO}_2$  prepared by refluxing method exhibit absorption at 285 nm, and the commercial P25 absorption at 330 nm, including the determined energy gaps ( $E_g$ ) at zero absorbance of 3.63 eV, 3.68 eV and 2.74 eV, respectively.

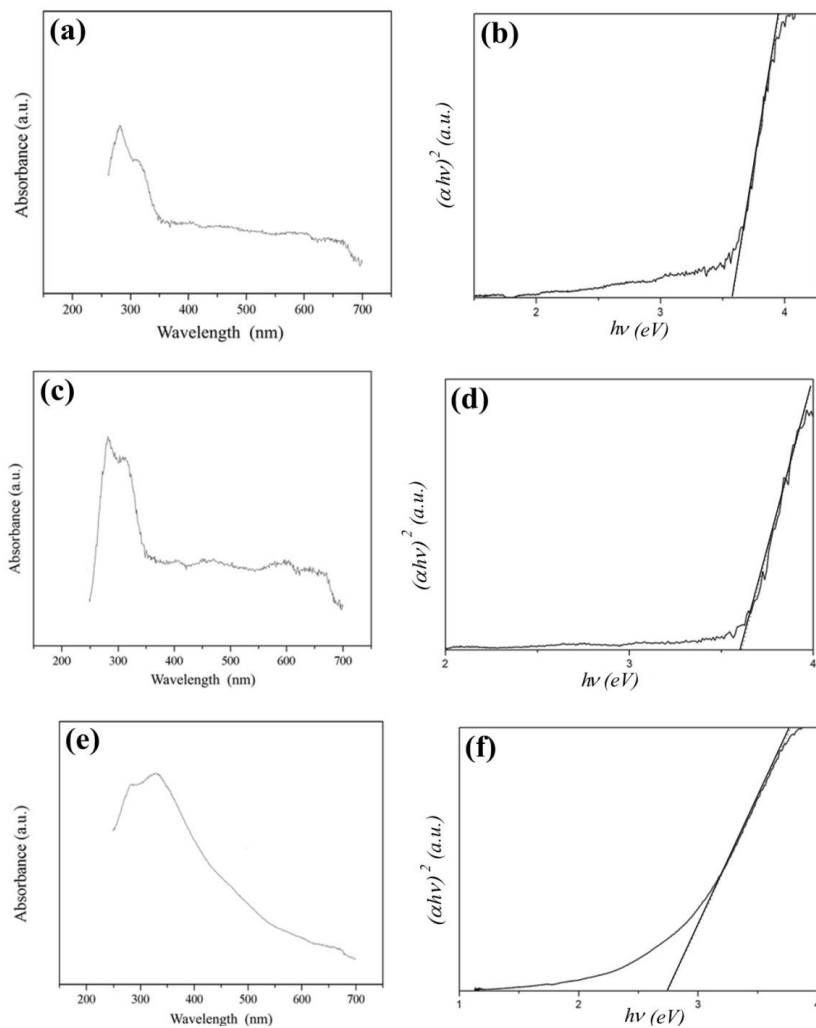


Fig. 6. The UV-vis absorption spectra of  $\text{TiO}_2$  nanopowders prepared by (a) sol-gel, (b) refluxing and (c) commercial P25.

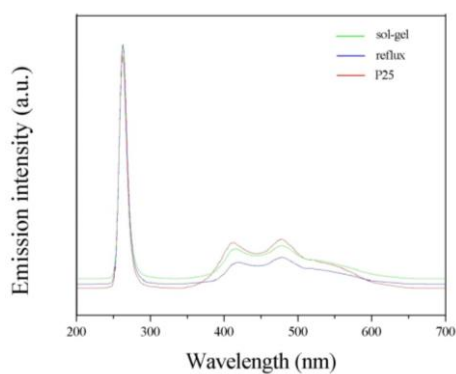


Fig. 7. PL spectra of  $\text{TiO}_2$  nanopowders prepared by sol-gel, refluxing and commercial P25 with 255 nm excitation wavelength at room temperature

The confirmation of these results has also been done with the help of PL spectroscopy. Fig. 7 shows PL spectra of  $\text{TiO}_2$  nanopowders prepared by sol-gel, refluxing and commercial P25 (excited by 315 nm wavelength) [18]. In this research, the emission peaks presented the band in the 200–700 nm range. When the current samples were excited by 255 nm wavelength, very close

to the wavelength at maximum absorption, their PL emission peaks were detected at the same value of 280 nm with some minor peaks at 415 and 480 nm.

### Photovoltaic performance

The photoelectric conversion efficiency was calculated according to the following

$$\eta\% = \frac{J_{sc} \times V_{oc} \times FF}{P_{in}} \times 100 \quad (2)$$

, where the fill factor (FF) is the ratio between the maximum output power density available ( $J_m V_m$ ) and the maximum power combining short-circuit and open-circuit situations. It describes the extent of square of the J–V curve according to the equation

$$FF(\%) = \frac{J_m \times V_m}{J_{sc} \times V_{oc}} \times 100 \quad (3)$$

, where  $J_{sc}$ ,  $V_{oc}$ , FF and  $P_{in}$  are the short-circuit current density, open-circuit voltage, fill factor and incident light power density, respectively [19-20]. To calculate the energy conversion efficiency of the as-fabricated solar cells using the deposited film of  $TiO_2$  aggregates of different sizes, the measurement of the current versus voltage under AM 1.5 simulated sunlight conditions of  $100 \text{ mW/cm}^2$  power density. The results are shown in Fig. 8 and the calculated characteristics parameters from the curves are presented in Table 1. The sensitization was achieved by the immersion of electrodes in the N719 solution for 30 min and 1 h. In this research, the  $V_{oc}$  was controlled by the immersion time to the highest value and then decrease. When the film was made of  $TiO_2$  nanopowder synthesized sol-gel method and soaked in N719 dye for 1 h, the efficiency of DSSC was the highest at 100 % for  $V_{oc} = 0.465 \text{ V}$ ,  $J_{sc} = 1.361 \text{ mA/cm}^2$  and  $FF = 0.647$ . The films was made of  $TiO_2$  nanopowder synthesized by refluxing method and soaked in N719 dye for 1 h, the efficiency of DSSC was at 81.37 % for  $V_{oc} = 0.410 \text{ V}$ ,  $J_{sc} = 1.287 \text{ mA/cm}^2$  and  $FF = 0.630$ . Two different films of  $TiO_2$  synthesized by sol-gel and refluxing methods, the efficiency was increased to highest for the 1 h immersion duration for the film of  $TiO_2$  with immersion time in N719 dye for 1 h, the longer time tended to be stationary. These results are very surprising if considering the fact that when increasing in the specific surface area, the amount of absorbed dye is increased and in turn the desensitization of the solar cell [19]. Furthermore, the dense film architecture is expected to facilitate better connectivity for efficient charge diffusion and limited recombination process. When the structure of the film is considered, some cracks were completely different for different films (Fig. 9). For cracked film, the conducting substrate intended to come into contact with oxidizing species in the electrolyte which enhance the recombination probability and in turn reduce the energy conversion efficiency of the solar cell. The cracks' connection will promote the formation of large dense domains which favor light scattering and harvesting. Additionally, the domain dense structure promotes the reduction of the electron path diffusion towards the substrate which can play the role in reducing the probability of recombination process [19].

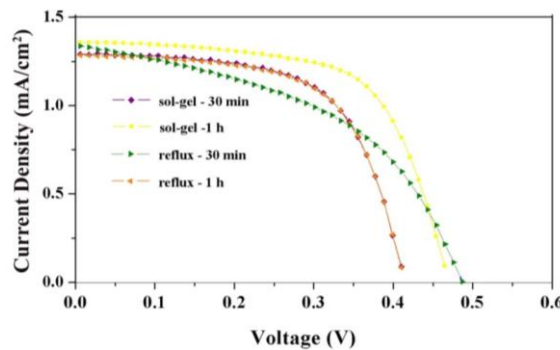


Fig. 8. Current density versus voltage of DSSCs made of different films synthesized by sol-gel and refluxing methods with 30 min and 1 h immersion under the AM 1.5 solar radiation.



Table 1. Calculated characteristic parameters

Sample	Immersion duration	$V_{oc}$ (V)	$J_{sc}$ (mA/cm <sup>2</sup> )	FF	$\eta$ (%)
Sol-gel	30 min	0.486	1.567	0.481	89.95
	1 h	0.465	1.361	0.647	100
reflux	30 min	0.487	1.346	0.472	75.73
	1 h	0.410	1.287	0.630	81.37

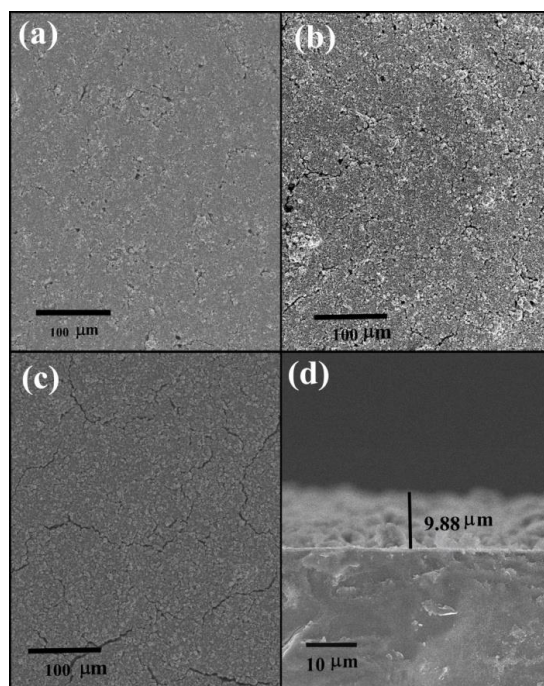


Fig. 9. FE-SEM images of  $TiO_2$  nanoparticles' films made of  $TiO_2$  synthesized by (a) sol-gel method, (b) reflux method, (c) commercial  $TiO_2$  (P25) and (d) cross section of the sol-gel film.

In case of the films of  $TiO_2$  nanoparticles synthesized by different methods, the characteristic cracks in terms of small width are both interconnected and isolated. The cracks did not promote electrical conductivity of photoactive film. Moreover, the film texture may result in lowering connectivity for effective charge diffusion between aggregates. All the phenomena mentioned above are attributed to reduce solar cell efficiency by lowering energy conversion. The crack-free structure of the film can prevent redox species in the electrolyte to come into contact with the conducting substrate and reduce the recombination probability, and lead to electrical disconnect of relevant part of photoactive film. According to the internal and surface morphology of the film synthesized by sol-gel, its efficiency is higher than the film synthesized by refluxing and the film of commercial P25.

#### 4. Conclusions

The successful synthesis of the pure titanium dioxide ( $TiO_2$ ) nanoparticles by sol-gel and refluxing methods is compared with commercial titanium dioxide (P25). All the samples were anatase phase and some amount of the rutile phase of  $TiO_2$ . The morphology of the samples containing spherical nanoparticles with the energy gap of the as synthesized  $TiO_2$  by sol-gel, refluxing method and commercial P25 were determined to be 3.63 eV, 3.68 eV and 2.74 eV, respectively. In this research, the performance of DSSCs showed that the higher energy conversion

efficiency of 100 % was achieved using the photoelectrode made of TiO<sub>2</sub> film synthesized by a sol-gel method.

### Acknowledgements

We wish to thank Thailand's Office of the Higher Education Commission for providing financial support through the National Research University (NRU) Project for Chiang Mai University (CMU), including the Faculty of Science of CMU, and the Graduate School of CMU through a general support.

### References

- [1] A.N. Banerjee, *Nanotechnol Sci Appl.* **4**, 35 (2011).
- [2] C. Su, B.-Y. Hong, C-M. Tseng, *Catal. Today* **96**, 119 (2004).
- [3] Y.S. Jin, K.H. Kim, H.W. Chol, S.J. Park, J.H. Kim, *J.Korean Phys. Soc.* **57**, 1049 (2010).
- [4] University of Toronto Scarborough. "Heating under reflux". [Online]. Available <http://webapps.uts.utoronto.ca/chemistryonline/reflux.php>. (2015, August 10).
- [5] P. B. Jimenez, Y. Yu, M.L. Cantu, C. Domingo, J. A. Ayllon, *J. Colloid Interface Sci.* **416**, 112 (2014).
- [6] B. Yacoubi, L. Samet, J. Bennaceur, A. Lamouchi, R. Chtourou, *Mater. Sci. Semicond. Process.* **30**, 361 (2015).
- [7] C. Henrist, J. Dewalque, F. Mathis, R. Cloots, *Microporous Mesoporous Mater.* **117**, 292 (2009).
- [8] A.R. Hernandez-Martinez, M. Estevez, S. Vargas, R. Rodriguez, *Composites Part B* **44**, 686 (2013).
- [9] H. Eskandarloo, A. Badiei. *Photocatalytic Application of Titania Nanoparticles for Degradation of Organic Pollutants*. Tehran: University of Tehran.
- [10] S. Bu, Z. jin, X. Liu, L. Yang, Z. Cheng, *Mater. Chem. Phys* **88**, 273 (2004).
- [11] O. Wiranwetchayan, W. Promnopas, K. Hongstith, S. Choopun, P. Singjai, S. Thongtem, *Res. Chem. Intermed* (2015) Accepted.
- [12] Powder Diffract. File, JCPDS-ICDD, 12 Campus Boulevard, Newtown Square, PA 19073-3273, USA, 2001.
- [13] L. Anicaia, A. Peticab, D. Patroic, V. Marinescuc, P. Prioteasac, S. Costovici, *Mater. Sci. Eng., B* **199**, 87 (2015).
- [14] S. Ananth, P. Vivek, T. Solaiyammal, P. Murugakoothan, *Optik* **126**, 1027 (2015).
- [15] N.-G. Park, J. van de Lagemaat, A. J. Frank, *J. Phys. Chem B* **104**, 8989 (2000).
- [16] M. Crisana, M. Raileanu, N. Dragana, D. Crisan, et al, *Appl. Catal. A: Gen.* (2014) 1-13.
- [17] A. Maurya, P. Chauhan, *Polym. Bull.* **68**, 961 (2012).
- [18] J. Sungpanich, T. Thongtem, S. Thongtem, *Ceram. Int.* **38**, 1051 (2012).
- [19] A. Taleb, F. Mesguich, A. Herissan, C. Colbeau-Justin, X. Yanpeng, P. Dubot, *Sol. Energy Mater. Sol. Cells* (2015)
- [20] W. Promnopas, T. Thongtem, S. Thongtem, *J Nanomater* (2014) Art ID: 529629, 6pp.